

## AN INNOVATIVE METHOD FOR MANUFACTURING $\gamma$ -TiAl FOIL

Stephen J. Hales<sup>1</sup>, Mohammad Saqib<sup>2</sup> and Joel A. Alexa<sup>2</sup>

<sup>1</sup>NASA Langley Research Center

<sup>2</sup>Lockheed Martin Engineering and Sciences Company  
MS 188A, 2 West Reid Street, Hampton, VA 23681, USA.

### Abstract

The manufacture and entrance into service of thin gage  $\gamma$ -TiAl product has been hampered by the inherent low room temperature ductility of the material. In the present study a new approach was explored for the efficient manufacture of  $\gamma$ -TiAl foil with improved ductility. The objective was to produce a very clean material (low interstitial content) with a highly refined, homogeneous microstructure placed in a fully lamellar condition. The processing route involved the use of RF plasma spray deposition of pre-alloyed powders, followed by consolidation via vacuum hot pressing and heat treatment. The approach took advantage of a deposition process which included no electrodes, no binders and high cooling rates. Results and discussion of the work performed to date are presented.

### Introduction

Over the past decade, a variety of ingot (IM) and powder metallurgy (PM) based processing routes have been devised to produce near-gamma titanium aluminide ( $\gamma$ -TiAl) alloy materials. The emphasis of alloy and process development has been on castings and forged components, primarily for propulsion applications [1]. More recently, there has been growing interest in the production of thin gage  $\gamma$ -TiAl materials for primary structure applications on high speed aircraft and reusable launch vehicles [2]. The recognized leader is Plansee AG, Austria, which has used a combination of IM and PM routes to manufacture sheet and foil products [3, 4]. The approach adopted utilizes multiple processing steps, including canning and de-canning activities, and tends to be expensive [1]. The primary objective of the present work is to take advantage of the microstructural refinement inherent to the direct metal deposition process to improve room temperature (RT) ductility. A secondary objective is to explore deposition processing technology for the more efficient production of  $\gamma$ -TiAl foil. Potential economic benefits stem from fewer processing steps and eliminating canning requirements.

The specific approach being adopted involves the use of low pressure, RF plasma spray deposition in combination with vacuum hot pressing and state-of-the-art heat treatment. Attractive features of this processing route include the absence of electrodes and binders, the inherent high solidification rates and the use of inert atmosphere throughout. This process culminates in as-deposited materials with highly refined microstructures and high purity (low interstitial content), both known to be beneficial to RT ductility [5]. Adjusting the deposition parameters to produce low-porosity deposits means that reduced time at temperature is warranted during secondary processing to effect complete consolidation. In contrast to many PM processes, the microstructural characteristics of the as-deposited material can be retained in the final product.

Extensive research effort has been devoted to establishing the processing-microstructure-property relationships in these alloys. Based on the best balance of strength, ductility and toughness at ambient and elevated temperatures a target multi-phase microstructure comprising the predominant  $\gamma$  (TiAl) phase and 5-25 %  $\alpha_2$  (Ti<sub>3</sub>Al) phase has been defined. The target microstructural condition comprises a grain size in the range 50-350  $\mu\text{m}$ , a fully lamellar microstructure with a fine inter-lamellar spacing ( $< 1 \mu\text{m}$ ) and serrated grain boundaries [5, 6]. This is typically achieved via a multi-step heat treatment practice comprising controlled heating into and hold in the  $\alpha+\gamma$  phase field, followed by controlled heating into and hold in the  $\alpha$  phase field and controlled cooling back through the  $\alpha+\gamma$  phase field into the  $\alpha_2+\gamma$  phase field [7].

Current commercial alloys tend to fall in the composition range (in at. pct.) Ti - Al<sub>45-48</sub> - (Cr,Mn,V)<sub>1-3</sub> - (Nb,W,Ta,Mo)<sub>1-5</sub> - (B,Si,C)<sub>0-1</sub>, where the Al content maximizes ductility for the binary alloy, (Cr,Mn,V) additions enhance RT ductility, (Nb,W,Ta,Mo) additions enhance high temperature properties and (B,Si,C) additions control grain size [3]. All of these solute additions cause subtle shifts in the key solvus temperatures for effective thermal processing into the desired microstructural condition. Therefore, the eutectoid temperature and the  $\alpha$  transus temperature need to be determined for a particular alloy [7]. The PM alloy used in this work ( $\gamma$ -MET) was developed by Plansee AG for wrought product and has the nominal composition Ti-46.5Al- 4.0(Cr,Nb,Ta,B) (in at. pct.) [3].

## Experimental Procedures

### Plasma Spray Deposition :

Figure 1(a) shows the RF plasma spray facility, which comprises a stationary plasma torch (hidden from view inside the Faraday cage) mounted on top of a cylindrical chamber and powered by an oscillator. The distinguishing features of this system are that it is a low pressure, electrodeless, low velocity device. The chamber is initially evacuated to a static vacuum of 1.33 Pa and maintained at a dynamic vacuum of 13.3 kPa during the deposition process. The plasma torch operating at 60 kW energizes an inductive coil to produce an RF magnetic field at a frequency of 400 kHz, Figure 1(b). This field couples with an argon/helium gas mixture, which is injected axially and tangentially into a quartz confinement tube surrounded by the coil. As the gases are ionized a plasma is generated which then exits through a water-cooled nozzle. The power, gas feed rate and dynamic vacuum control the plasma temperature and the size, shape and velocity of the plasma plume.

The pre-alloyed  $\gamma$ -TiAl powder feedstock, sieved to  $-80 +140$  mesh (100-180  $\mu\text{m}$  diameter) range, was provided by Crucible Research, Inc., PA. The powder is transported from feeders to the plasma torch by a carrier gas (helium) at a controlled rate and is injected axially via a water cooled injection probe located directly above the plasma. The powder travels through the plasma, melts and is accelerated through an exit nozzle toward a rotating, translating mandrel, Figure 1(c). The mandrel is a 30.5 cm diameter x 30.5 cm long water-cooled steel cylinder covered with a sacrificial mild steel foil substrate. The droplets impinge and solidify on the substrate in a helical pattern and the deposit thickness is controlled via the deposition time. Periods of pre- and post-heating of the substrate using the plasma are imposed during the process to improve deposition efficiency (adhesion) and relieve residual stresses, respectively. The baseline parameters employed to plasma spray the  $\gamma$ -TiAl powders are listed in Table 1. Upon removal from the mandrel, a typical deposit (plus substrate foil) is 15.2 cm wide by 91.4 cm long. This is then sectioned into sheets of suitable size for vacuum hot pressing (7.6 cm x 12.7 cm). The substrate foil is then removed via chemical milling using a 50 % nitric acid-50 % water solution and the remaining deposit is bright dipped in a 44 % nitric acid, 6 % hydrofluoric acid and 50 % water solution to remove any residuals.

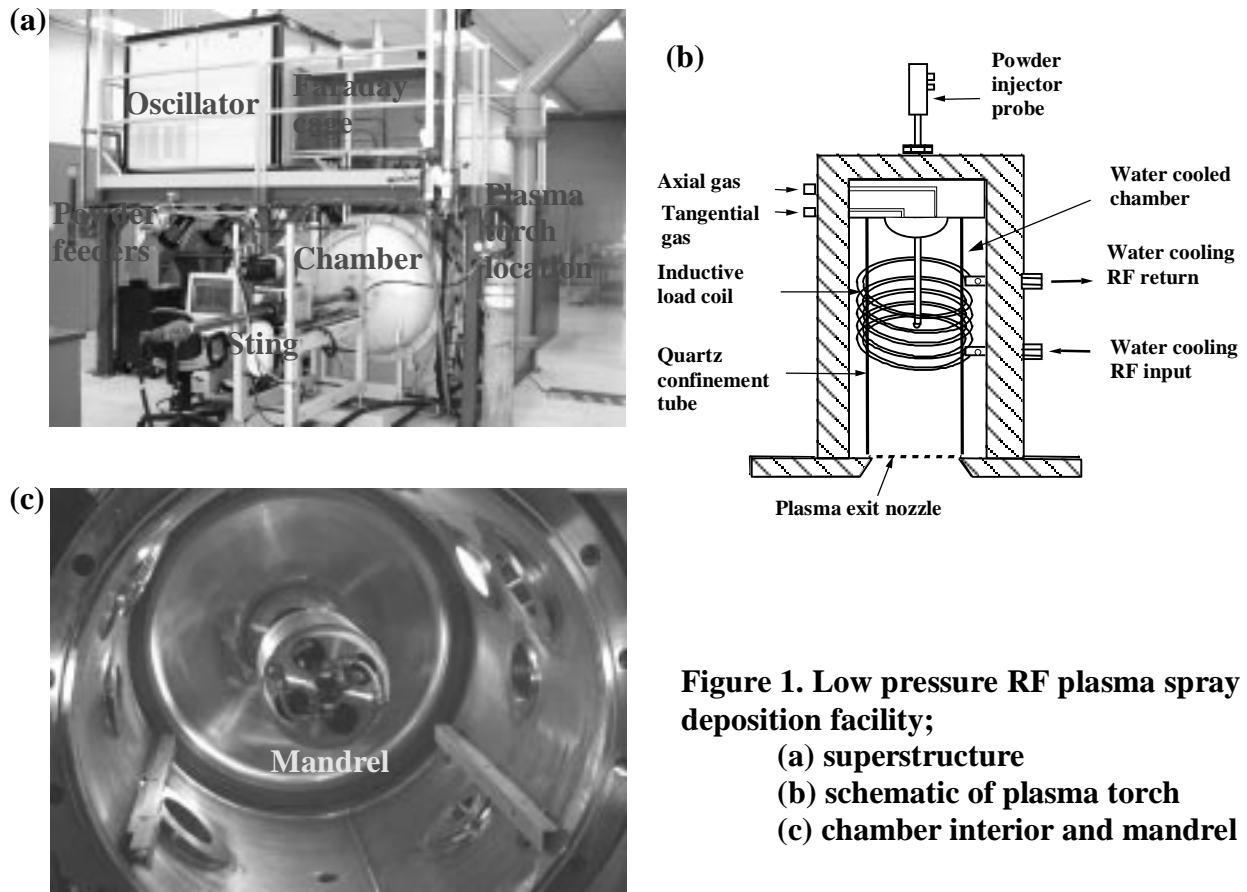


**Figure 1. Low pressure RF plasma spray deposition facility;**

- (a) superstructure**
- (b) schematic of plasma torch**
- (c) chamber interior and mandrel**

**Table 1. RF plasma spray deposition parameters.**

<b>Parameter:</b>	<b>Value:</b>	<b>Notes:</b>
Voltage	6 kV	
Current	10 amps	
Dynamic chamber vacuum	13.3 kPa	
Argon/Helium flow rate	160 l/min.	
Argon/Helium gas mix ratio	3:2	
Axial/tangential gas mix ratio	5:3	
Nozzle to target distance	50.8 cm	
Powder feed rate	25 g/min.	
Carrier gas flow rate	5 l/min.	helium
Mandrel rotation speed	35 rpm	for 30.5 cm diameter
Mandrel translation speed	5.1 cm/sec	over 20.3 cm for 15.2 cm wide target
Pre-heat time	3 min.	
Deposition time	10 min.	
Post-heat time	5 min.	controlled heat decay

#### VHP Consolidation :

The vacuum hot press (VHP) facility has a load capacity of 172 tonnes (190 tons) applied to 30.5 cm diameter molybdenum platens and can be operated in load or stroke control, Figure 2(a). The VHP operates at temperatures up to 1200°C and a vacuum level in the  $10^{-3}$  to  $10^{-4}$  Pa range. Multiple plies (up to 6) of as-deposited material were layed-up in a 12.7 cm x 7.6 cm molybdenum die which was coated with boron nitride as a release agent, Figure 2(b). Parametric studies were conducted at temperatures ranging from 800°C to 1100°C and

pressures ranging from 103 MPa to 172 MPa using a consolidation time of 2 hrs. The goal was to employ the lowest temperature at which complete consolidation occurred in order to minimize microstructural coarsening effects. The VHP cycle selected for this work comprised 900°C / 138 MPa / 2 hrs and a typical thermal and load profile is shown in Figure 2(c). Relieving the load prior to cooling below 700°C was found to be critical to avoid cracking.

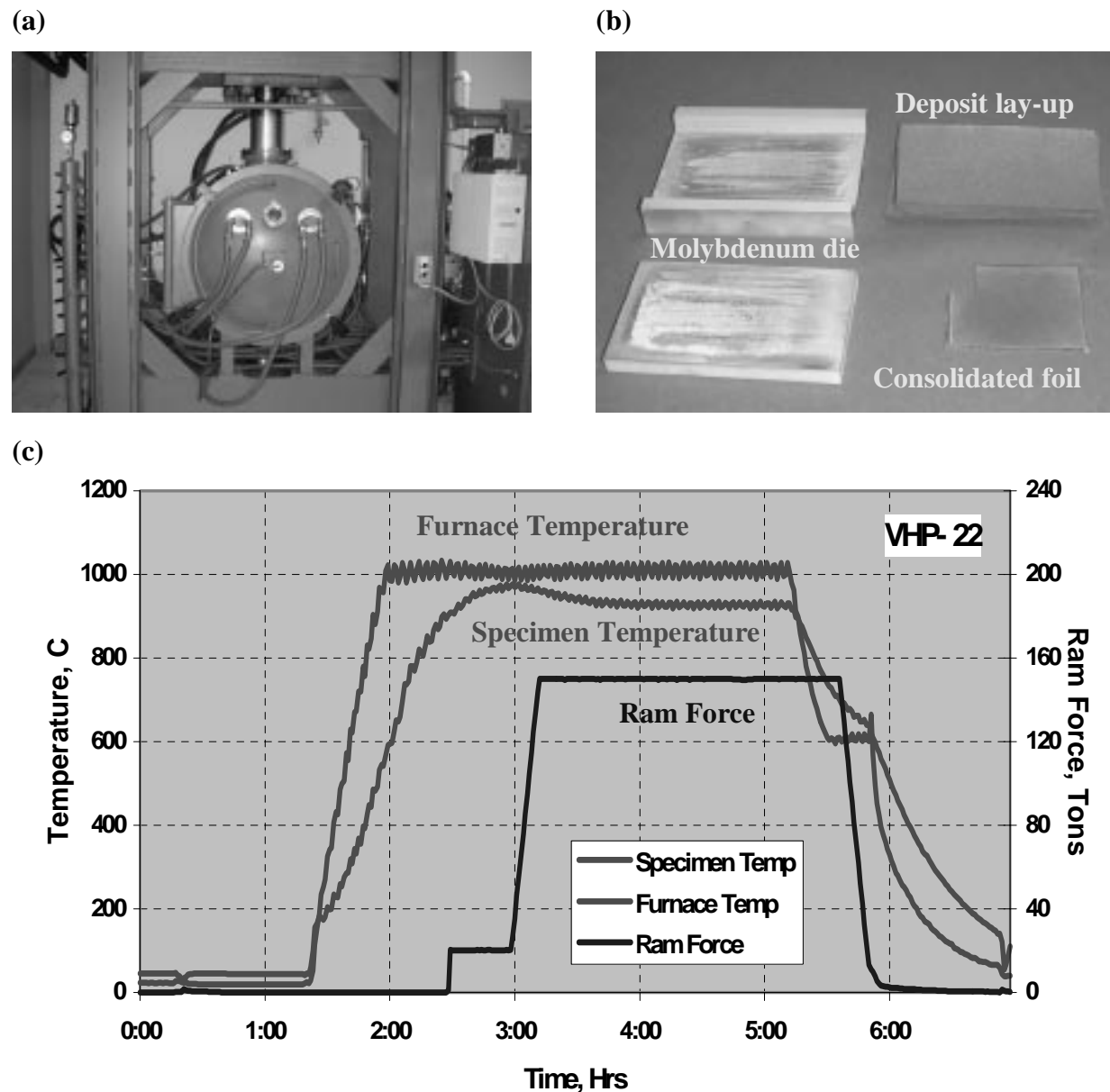


**Figure 2. Vacuum hot press facility;** (a) superstructure  
(b) molybdenum die and deposit lay-up  
(c) typical temperature / load profile

#### Heat Treatment :

After electro-machining standard ASTM E8 tensile blanks from the as-consolidated material, coupons were extracted from the scrap for parametric heat treatment studies, Figure 3(a). The coupons were wrapped in tantalum foil and encapsulated in quartz tubes which were evacuated and back-filled with a partial pressure (13.3 Pa) of ultra-pure helium gas. It was determined that this pressure would increase to just below atmospheric (93.1 kPa) at the highest heat treatment temperatures employed. The thermal profile for a typical multi-step heat treatment cycle is shown in Figure 3(b). The profile shows the furnace temperature as a function of time.

For this particular practice, the two ‘blips’ on the plot are related to the opening of the furnace to insert and remove the specimens, respectively. The first stage is a homogenization heat treatment, involving a ramp and holding period in the  $\alpha+\gamma$  phase field. The second stage is a transformation heat treatment, involving a ramp and holding period in the  $\alpha$  phase field. The third stage involves controlled cooling through the  $\alpha+\gamma$  phase field to produce a fully lamellar  $\alpha_2+\gamma$  microstructure. The cooling rate from the  $\alpha$  transus to approximately 1150°C is deemed critical in controlling the mode of transformation and the  $\alpha_2+\gamma$  inter-lamellar spacing.

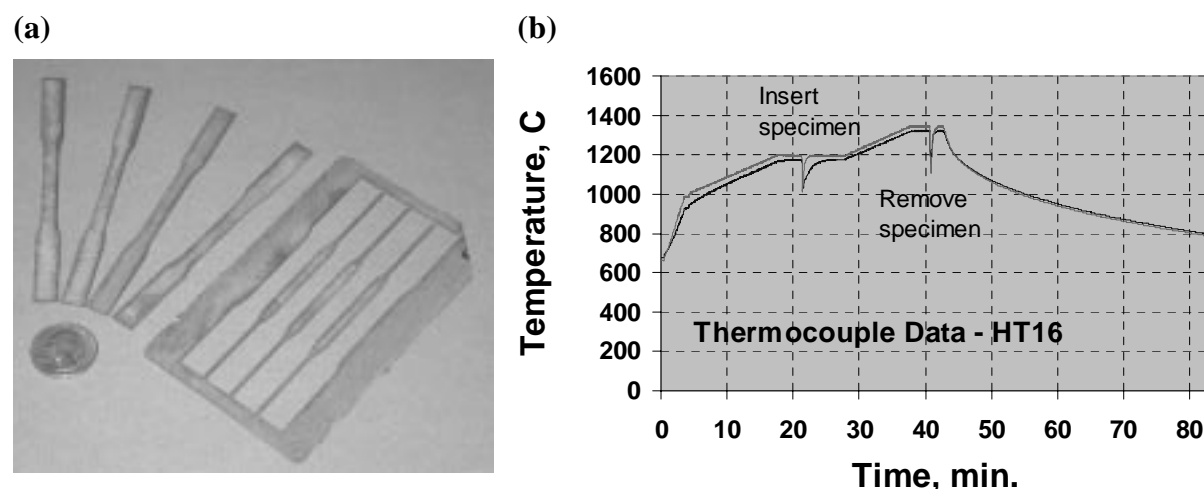


**Figure 3. Heat treatment studies; (a) consolidated panel + tensile blanks (b) typical thermal profile**

Parametric studies were conducted which addressed all three stages of the heat treatment independently. Again, the objective was keeping ‘time at temperature’ to a minimum in order to minimize microstructural coarsening effects. Based on a pseudo-binary phase diagram and following the work of others, the eutectoid and  $\alpha$  transus temperatures for this alloy were estimated to be 1125°C and 1315°C, respectively. For the first stage the heating rate was either 90°C/min. to 1000°C followed by 15°C/min. to 1200°C or rapid heating (> 400°C/min.) by placing samples in a furnace preheated to 1200°C. The holding period at 1200°C comprised times ranging from 1 to 20 minutes. For the second stage, the heating rate was 15°C/min. to temperatures ranging from 1300°C to 1350°C and the holding time ranged from 1.5 to 50 min. The target for the second stage was heat treatment at 10° to 20°C above the  $\alpha$  transus temperature. For the third stage, cooling rates to 1150°C varied from furnace cooling (70°C/min.) to air cooling (25-30°C/sec).

#### Mechanical Testing :

Room temperature mechanical testing was conducted in accordance with ASTM E8 specifications using standard sub-size tensile specimens. The stroke rate was 0.013 cm/min. and strain was measured across a 2.54 cm gage length using back-to-back extensometers.

### **Results and Discussion**

#### Plasma Spray Deposition :

Two key objectives for parameter selection for plasma spray deposition were to retain the starting alloy composition and minimize interstitial contamination. The composition of the as-spray deposited material is compared with that of the as-received powder in Table 2. The results show that the solute content is unchanged (within experimental error) and that there has been a slight increase in interstitial content with the exception of hydrogen. Other studies of

plasma spray deposition of TiAl-based alloys have reported high levels of contamination with N and O resulting in the formation of nitrides and oxides and a significant reduction in mechanical properties [8]. The deposited material from a single plasma spray run was used exclusively for the consolidation and heat treatment studies.

**Table 2. Compositional variations during processing (in wt. pct.).**

Element	Starting powder	As-deposited LPS-21	As-consolidated VHP-22
Ti	Bal.	Bal.	Bal.
Al	33.0	32.8	32.3
Cr	2.8	3.4	3.5
Nb	2.6	2.6	2.6
Ta	2.5	2.4	2.5
B	0.031	0.026	0.030
O	0.065	0.112	0.120
C	0.021	0.032	0.032
N	0.008	0.015	0.013
H	0.0046	0.0014	0.0009

Comparisons between the microstructural features of the powder feedstock and the plasma sprayed material permits evaluation of the degree of melting during the deposition process. A target of 100 % melting is usually preferable, but other factors such as loss of fugitive elements (Al) and minimizing interstitial content had to be considered. Therefore, following empirical studies the plasma spray parameters adopted here represented a compromise on this basis. Figure 4(a) shows that although most of the powders are close to spheroidal in shape, some powder morphologies include irregular shapes, satellites and splats. The microstructure of the powders is consistent throughout comprising a dual phase ( $\alpha_2 + \gamma$ ) as-solidified structure typical of spray-atomized material. A representative section of 0.36 mm thick plasma spray deposited material is shown in Figure 4(b). The microstructural features indicate that most of the powders have melted to form a featureless rapidly solidified structure (see A). However, some powders have only partially melted and been deformed while retaining remnants of the original microstructure (see B), and others have remained un-melted and retained both shape and microstructure (see C). The level of porosity present (estimated at 50 %) is typical of low velocity plasma sprayed material and is removed during secondary consolidation.

#### VHP Consolidation :

The composition of the as-consolidated material is compared with that of the as-deposited material in Table 2. The results show that the solute content is still unchanged and that there has been a further slight increase in interstitial content with the exception of hydrogen. These increases are below the limits set forth by many researchers as threshold values for causing deterioration in mechanical properties [5]. Figures 5(a)-(c) show vacuum hot pressed material in the form of three 7.6 cm x 12.7 cm panels with final gages of 0.76 mm, 0.51 mm and 0.30 mm. These panels were the result of consolidating lay-ups of six, four and two 0.36 mm thick plies of deposited material, respectively. Figures 5(a)-(c) also show these panels in full thickness cross-section where some surface roughness can be observed. The reduction in thickness during consolidation varies between 57 % (2-ply) and 64 % (4- and 6-ply). The materials are uniform and free from cracks but there was evidence of a small amount of macro-porosity (< 0.1 %). Figure 5(d) shows the representative microstructure in more detail. The microstructure comprises a homogeneous, dual phase  $\alpha_2 + \gamma$  structure with a highly refined grain size estimated at 5  $\mu\text{m}$ .

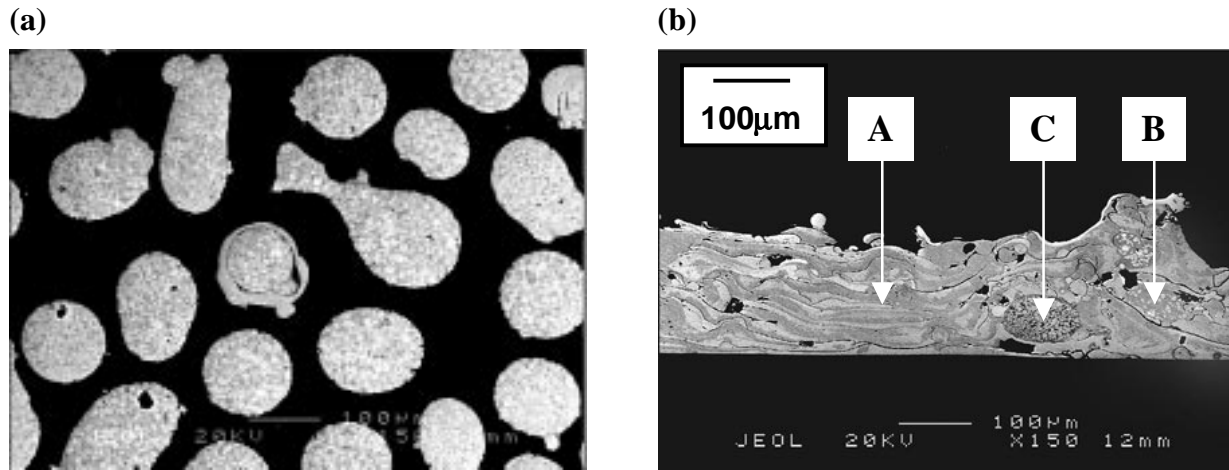


**Figure 4. SEM backscattered electron images; (a) starting  $-80 +140$  mesh powders (b) as-plasma spray deposited**

#### Heat Treatment :

Many different heat treatment cycles were attempted with an emphasis on keeping the time at temperature as short as possible to achieve the finest microstructure, but still long enough to get complete homogenization and promote the desired phase transformations. The results of employing the different heat treatment routines are summarized in Table 3. The microstructural characteristics listed reflect the results of SEM observation of all of the heat-treated specimens and some representative images are shown in Figure 6. It was determined from these observations that the second stage heat treatment must be conducted above the  $\alpha$  transus temperature and the critical cooling rate during the third stage heat treatment to form a lamellar microstructure in this alloy must be higher than  $30^{\circ}\text{C}/\text{min}$ .

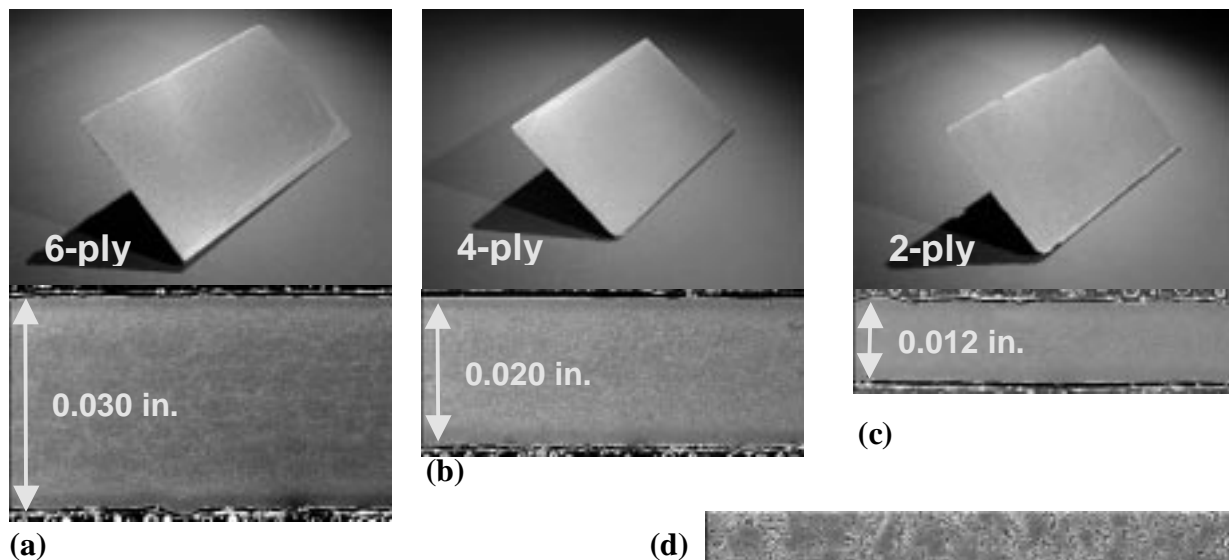


**Figure 5. As-consolidated 7.6 cm x 12.7 cm panels;**  
 (a) 6-ply; 0.76 mm thick  
 (b) 4-ply; 0.51 mm thick  
 (c) 2-ply; 0.30 mm thick  
 (d) representative microstructure

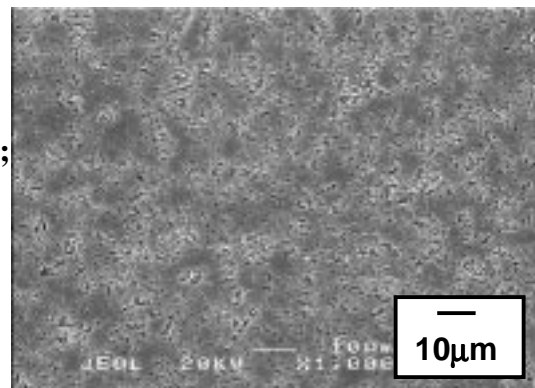


**Table 3. Effect of heat treatment practice on microstructure.**

Spec. ID	Heat Treatment						Microstructural Characteristics				
	Stage 1		Stage 2		Stage 3	Notes	Amt. Lam. %	Lam. Col. Size $\mu\text{m}$	Equi-axed $\gamma$ size $\mu\text{m}$	Inter-Lam. Spacing $\mu\text{m}$	GB Char.
	Temp. $^{\circ}\text{C}$	Time min.	Temp. $^{\circ}\text{C}$	Time min.	Cooling Rate $^{\circ}\text{C}/\text{min.}$						
HT04	1200	20	1320	15	50	A	85	50-100	5-10	2-5	P
HT05	1200	20	1300	15	50	A	0	NA	5-10	NA	P
HT06	1200	10	1300	15	50	A	0	NA	5-10	NA	P
HT07	1200	10	1320	15	50	A	50	50	5-10	2-5	P
HT08	1000	20	1320	5	AC	A	100	50-100	NA	1	S
HT09	NA	NA	1320	3	70	A	40	20-40	10	1	P
HT11	NA	NA	1320	3	30	C	5	20-40	10	2-5	P
HT12	NA	NA	1325	3	AC	A	95	10-50	5	0.5-1	S
HT13	NA	NA	1315	8	AC	C	70	10-50	5	0.5-1	S+P
HT14	1200	5	1325	5	70	A	95	50	10	2-5	P
HT15	1200	5	1310	4	AC	B	80	20-40	10	0.2-0.5	S+P
HT16	1200	5	1340	3	AC	B	100	20-50	NA	0.5-1	S
HT17	1200	3	1330	3	AC	B	95	10-40	5	0.2-0.5	S+P
HT18	1200	1	1335	1.5	AC	B	95	10-40	5	0.2-0.5	S+P
HT19	NA	NA	1330	1.5	AC	C	0	NA	5	NA	P

NA = Not applicable or none

Stage 1; heating rate =  $90^{\circ}\text{C}/\text{min.}$  to  $1000^{\circ}\text{C}$  +  $15^{\circ}\text{C}/\text{min.}$  to  $1200^{\circ}\text{C}$  or  $> 400^{\circ}\text{C}/\text{min.}$

Stage 2; heating rate =  $15^{\circ}\text{C}/\text{min.}$

Stage 3; AC = air cooled ( $25\text{-}30^{\circ}\text{C}/\text{sec}$ )

A = specimen inserted in the furnace at RT

B = specimen inserted in the furnace at stage 1 aging temperature

C = specimen inserted in the furnace at stage 2 aging temperature

P = planar grain boundaries

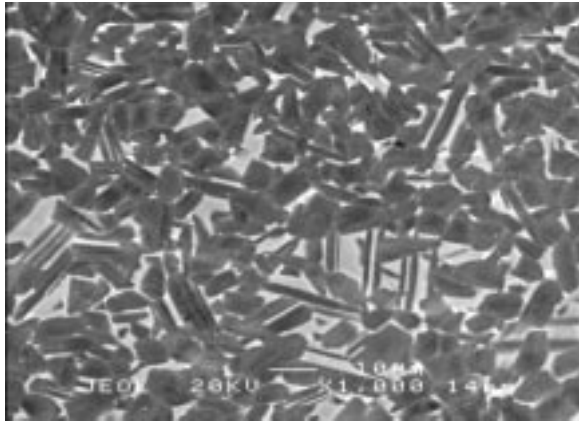
S = serrated grain boundaries

Figure 6(a) shows that specimens cooled slower than the critical rate (HT11) form an equiaxed, dual phase microstructure comprising fine  $\alpha_2$  and  $\gamma$  grains. These are known to form via a cellular reaction, with little or no lamellar microstructure formation [5, 6, 7]. When the cooling rate is above the critical rate required to form a lamellar microstructure, the inter-lamellar spacing is proportional to the cooling rate. For example, specimens cooled at  $70^{\circ}\text{C}/\text{min.}$  (HT14) had much coarser lamellae as compared to the air-cooled ( $25\text{-}30^{\circ}\text{C}/\text{sec}$ ) specimen (HT16). This is observed by comparing Figure 6 (c) and Figure 6(d). Heat treatment practice HT16 produced a fully lamellar microstructure with a colony size of  $20\text{-}50\ \mu\text{m}$  and an inter-lamellar spacing of  $0.5\text{-}1.0\ \mu\text{m}$ . It should be noted that faster rates than can be achieved via air cooling are considered impractical for thin gage materials due to residual quench stresses.

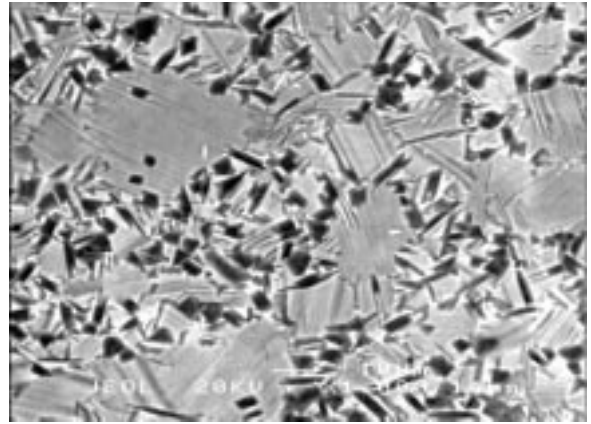
A variety of microstructures can be engineered by making small changes to aging times and temperatures in the two-step heat treatment. During the first stage of heat treatment (at  $1200^{\circ}\text{C}$ ) the microstructure consists of large  $\alpha$  grains and fine  $\gamma$  grains. When heated to the second aging temperature above the  $\alpha$  transus, the  $\gamma$  grains are dissolved to form the single  $\alpha$  phase [7]. Partial dissolution of  $\gamma$  grains can be attained by reducing the aging time and/or temperature and then air-cooling (HT13). The microstructures generated in this manner comprise colonies of lamellae with fine  $\gamma$  grains (about  $5\ \mu\text{m}$ ) decorating the inter-colony boundaries (see Figure 6(b)). Previous work has shown that the volume fraction of these fine  $\gamma$  grains can be engineered to tailor the strength and toughness of these types of alloys [5, 6, 7].



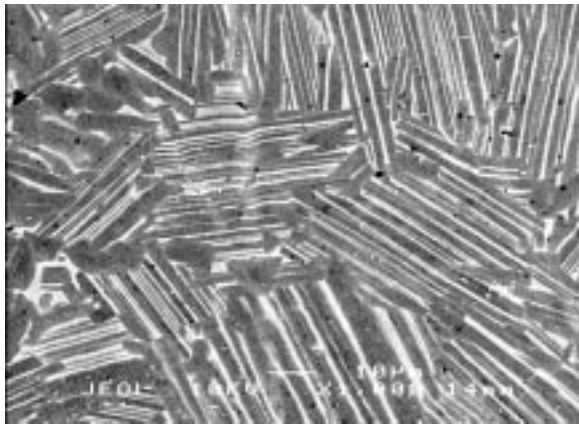
(a)



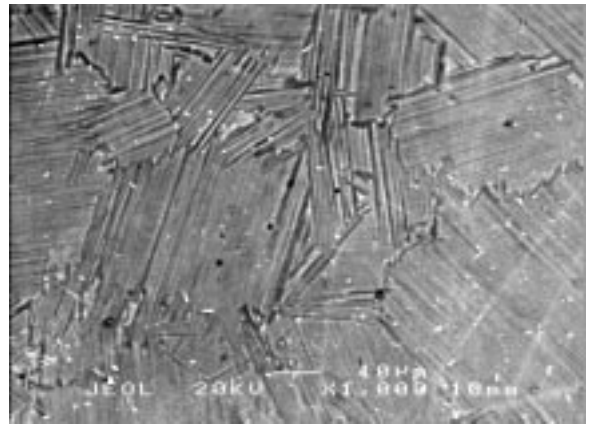
(b)



(c)



(d)



—  
10μm

**Figure 6. Microstructures following heat treatment;**

- (a) equiaxed  $\alpha_2$  plus  $\gamma$  grains (HT11)**
- (b) fine lamellar plus fine equiaxed  $\gamma$  grains (HT13)**
- (c) coarse fully lamellar grain structure (HT14)**
- (d) fine fully lamellar grain structure (HT16)**

**Mechanical Testing :**

The objective of this research was to generate a microstructure most suitable for enhanced room temperature ductility. As noted from the research of others and discussed earlier, a fine fully lamellar grain structure with serrated grain boundaries is the target microstructural condition. Therefore, the heat treatment parameters shown for practice HT16, which resulted in the microstructure shown in Figure 6(d), were employed for the mechanical test specimens. Specimens were placed in the furnace at 1200°C, held for 5 min., furnace heated to 1340°C, held for 3 min. and air cooled. Table 4 shows the results of these tests compared with typical tensile properties of  $\gamma$ -MET sheet processed by more conventional means (with a coarser fully lamellar grain structure) [3]. Although the processing route in the present work has not been optimized, the yield strength is higher, probably as a result of the finer lamellar grain structure, and the RT ductility is lower, probably due to surface roughness and residual macro- and micro-porosity (Figure 5). Parametric studies to improve VHP consolidation practices, while minimizing microstructural coarsening effects, will be the focus of future work.

**Table 4. Room temperature tensile data.**

Spec. ID	# plies	E GPa	UTS MPa	YS MPa	$e_p$ %	$e_{tot}$ %	Notes
MHT 2-1	2	150	342	---	0.04	0.27	A, B
MHT 1-2	4	159	531	494	0.30	0.63	A
MHT 2-2	4	160	491	487	0.21	0.52	
MHT 1-3	6	165	535	508	0.33	0.65	
MHT 2-3	6	164	462	---	0.12	0.40	A
Average	---	162	505	496	0.24	0.55	
Ref. 3	---	169	484	397	---	1.40	

*All materials in fully lamellar microstructural condition*

*Modulus calculated from 0 to 0.1 % strain*

*A = specimens broke outside of the gage length*

*B = data not included in determination of average values*

## Conclusions

1. Plasma spray deposition produced 0.36 mm thick plies of  $\gamma$ -TiAl material with alloy composition close to the starting powders, including low interstitial content. The majority of powders were melted during the process and the as-deposited porosity level was approximately 50 %.
2. Vacuum hot press consolidation resulted in a greater than 50 % reduction in thickness of 2-, 4-, and 6-ply materials and a retention of alloy composition with the exception of a slight increase in oxygen content. The residual porosity level was reduced to < 0.1%.
3. Heat treatment studies resulted in a fine-grained ( $d = 20\text{--}50\ \mu\text{m}$ ), refined fully lamellar ( $\lambda = 0.5\text{--}1.0\ \mu\text{m}$ ) microstructure with serrated grain boundaries when specimens were placed in the furnace at 1200°C, held for 5 min., furnace heated to 1340°C, held for 3 min. and air cooled.
4. The strength of the RF plasma spray deposited and VHP consolidated materials compared favorably with the tensile properties of  $\gamma$ -MET sheet processed via more conventional means. RT ductility will be improved by adjusting processing parameters to reduce surface roughness and eliminate macro- and micro-porosity.

## References

1. S.L. Semiatin et al., in *Structural Intermetallics 1997*, M.V. Nathal et al. (eds.), TMS, Warrendale, PA, 1997, pp. 263-276.
2. P.A. Bartolotta and D.L. Krause, in *Gamma Titanium Aluminides 1999*, Y.-W. Kim, D.M. Dimiduk and M.H. Loretto (eds.), TMS, Warrendale, PA, 1999, pp. 3-10.
3. R. LeHolm, H. Clemens and H. Kestler, in *Gamma Titanium Aluminides 1999*, Y.-W. Kim, D.M. Dimiduk and M.H. Loretto (eds.), TMS, Warrendale, PA, 1999, pp. 25-33.
4. H. Clemens et al., in *Structural Intermetallics 1997*, M.V. Nathal et al. (eds.), TMS, Warrendale, PA, 1997, pp. 277-286.
5. Y.-W. Kim, J. Mater.Sci.Eng., vol.A192/3, 1995, pp. 519-533.
6. C.T. Liu et al., J. Intermetallics, vol.4, 1996, pp. 429-440.
7. D.M. Dimiduk et al., J. Mater.Sci.Eng., vol.A243, 1998, pp. 66-76.
8. K. Honda, A. Hirose and H. Kobayashi, J. Mater.Sci.Eng., vol.A222, 1997, pp. 212-220.

## Acknowledgements

Photographic support from Mr. Jim Baughman of Lockheed Martin Engineering and Sciences Company, Hampton, Virginia, is greatly appreciated.